Int. J. Heat Mass Transfer. Vol. 19, pp. 355–366. Pergamon Press 1976. Printed in Great Britain

ANALYSIS OF SURFACE TENSION DRIVEN FLOW IN FLOATING ZONE MELTING

CHONG E. CHANG and WILLIAM R. WILCOX*
Chemical Engineering and Materials Science Departments, University of Southern California, Los Angeles, CA 90007, U.S.A.

(*Received* 1 *August* 1974 *and in revised form* 7 *July* 1975)

Abstract—Surface tension driven flow in a cylindrical melt suspended between two rods was investigated by numerical solution of the steady state differential equations for heat and momentum transfer Radiation heating and electron beam heating were considered approximately. For small values of the driving force, one rotating ring was formed in the top half of the zone, and its mirror image in the bottom half. At larger driving forces, secondary cells form which probably would undergo oscillatory motion. The influence of Prandtl number, zone movement, and buoyancy on the convection was also studied. The primary resistance to mass transfer in the laminar regime was in the center of the zone rather than at the solid–liquid interfaces.

NOMENCLATURE

a, radius of the molten zone [cm];
C_p, specific heat of melt [cal/g°K];
D, binary molecular diffusion coefficient [cm^2/s];
g, acceleration [cm/s^2];
Gr_h, Grashof number for heat transfer $[g\beta(T_0-T_m)a^3/\nu^2]$;
Gr_m, Grashof number for mass transfer $[g\alpha w_0 a^3/\nu^2]$;
i, integer denoting grid station in axial direction, $i = 1, 2, 3, \ldots, m$;
j, integer denoting grid station in radial direction, $j = 1, 2, 3, \ldots, n$;
k, thermal conductivity of melt [cal/cm s°C];
k_0, interfacial distribution coefficient, w_0/w at freezing interface ($z = -l$);
l, one-half of the liquid zone length [cm];
m, integer denoting the last grid station in axial direction;
M, dimensionless surface tension parameter at the free melt surface $\rho_f a(T_0-T_m)(\partial\gamma/\partial T)/\mu^2$;
Ma, Marangoni number, $(\partial\gamma/\partial T)qa^2\rho_f C_p/k^2\mu$;
n, integer denoting the last grid station in radial direction;
P, pressure in the melt;
Pr, Prandtl number, $\mu C_p/k$;
q, heat transferred from heater to zone;
r, radial coordinate, measured from the center of the zone [cm];
R, dimensionless radial coordinate, r/a;
Sc, Schmidt number, $\mu/\rho_f D$;
T, temperature [°K];
T_c, temperature of surroundings [°K];
T_0, temperature at $r = a$, $z = 0$ [°K];
T_m, interfacial temperature (melting point) [°K];
ΔT, (T_0-T_m);
v_c, zone travel rate (taken to be positive in the z direction) [cm/s];
v_r, radial velocity component of the melt [cm/s];
v_z, axial velocity component of the melt [cm/s];
V_c, dimensionless zone travel rate, $v_c a/\nu$;
V_r, dimensionless radial velocity component of the melt, $v_r a/\nu$;
V_z, dimensionless axial velocity component of the melt, $v_z a/\nu$;
w, weight fraction impurity in melt at z and r;
w_0, weight fraction impurity in feed, assumed uniform;
w_c, weight fraction impurity in product at r;
z, axial coordinate, measured from the center of the zone [cm];
Z, dimensionless axial coordinate, z/a.

Greek symbols

α, $(\partial\rho_f/\partial w)/\rho_f$;
β, $(\partial\rho_f/\partial T)/\rho_f$;
γ, surface tension between melt and vapor [dyne/cm];
ε_s, emissivity of thermal radiation;
θ, dimensionless temperature, $(T-T_m)/\Delta T$;
θ_c, dimensionless temperature of the surroundings, $(T_c-T_m)/\Delta T$;
μ, viscosity of the melt [g/cm s];
ν, kinematic viscosity, μ/ρ_f [cm^2/s];
ρ_c, density of the crystal [g/cm^3];
ρ_f, density of the melt [g/cm^3];
σ, Stefan–Boltzmann constant, $5{\cdot}668\times10^{-5}$ [erg/cm^2 s°K^4];
Φ, dimensionless impurity concentration, w/w_0;
ψ, dimensionless stream function, defined such that $V_r = \frac{1}{R}\frac{\partial\psi}{\partial Z}$ and $V_z = -\frac{1}{R}\frac{\partial\psi}{\partial R}$;
ω, dimensionless vorticity, $= \frac{\partial V_r}{\partial Z}-\frac{\partial V_z}{\partial R} = \frac{1}{R}\left(\frac{\partial^2\psi}{\partial R^2}-\frac{1}{R}\frac{\partial\psi}{\partial R}+\frac{\partial^2\psi}{\partial Z^2}\right)$.

*Present address: Department of Chemical Engineering, Clarkson College of Technology, Potsdam, N.Y. 13676.

INTRODUCTION

FLOATING zone melting is used commercially and in research for crystal growth and for purification of high melting materials [1, 2]. The melt does not contact a crucible, as shown schematically in Fig. 1. The melt is held by surface tension forces in opposition to gravity,

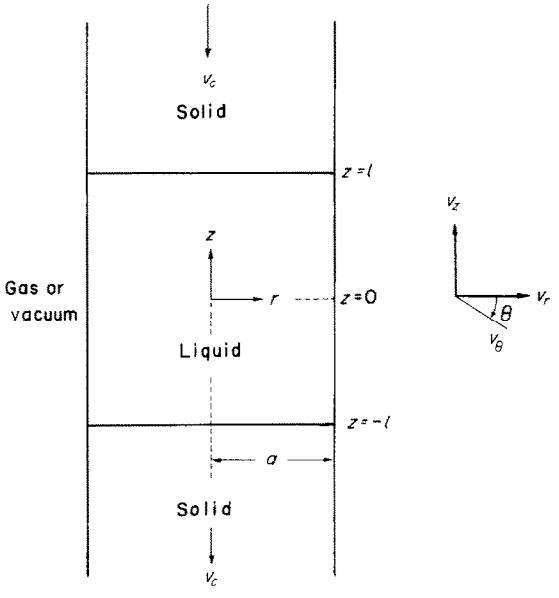

FIG. 1. Geometry, coordinate system and fluid velocity components for floating zone melting.

thereby limiting the possible diameter of the zone on earth. Heating may be by radiation, by an electron beam, or by induction from a surrounding high frequency coil. The zone is moved through the solid either by moving the heater or by moving the solid rods bordering the zone. There are five sources of convection in a floating zone:

(1) When the zone is taken as stationary, there is a flow through the zone generated by melting at one solid–liquid interface and freezing at the other, due to movement of the zone through the solid [3].

(2) Convection due to rotation of the two solid rods. (Slow rotation is sometimes used to maintain a cylindrical zone and growing rod.)

(3) With induction heating one obtains electromagnetic stirring, which is probably impossible to calculate.

(4) Buoyancy-driven natural convection due to interaction of a gravitational or accelerational field with density variations in the melt caused primarily by temperature variations.

(5) Surface-tension driven flow due to variations in surface tension along the melt surface caused primarily by the variation in temperature along the surface.

Because of the probable exploitation of this process in space, we were particularly interested in convection in the absence of gravity (4).

The purpose of the calculations described here was to estimate the magnitude of the surface-driven (Marangoni) flow and its influence on heat and mass transfer. Mass transfer influences the degree of purification and the homogeneity of single crystals. Heat transfer influences the perfection of the crystals, the stability of the zone, and sometimes influences the homogeneity as well, through its effect on the freezing interface shape. In order to determine the influence of surface driven flow on zone melting, the partial differential equations for momentum and heat transfer were considered. Solutions were obtained numerically for two situations—a parabolic temperature profile along the melt–vapor surface and for a ring heat source at the center of the zone. The parabolic temperature profile corresponds approximately to radiant heating, and the ring source corresponds to electron beam heating. The mass-transfer equation coupled with the computed flow fields were employed to find the impurity concentration fields in the melt at steady state.

The results of the calculations are expressed in dimensionless form and for the physical properties of silicon with a 1×1 cm zone, as a concrete example. For molten silicon the melting point is 1410°C, the Prandtl number is 0·023, the Schmidt number is about 5, $\rho_f(\partial\gamma/\partial T)/\mu^2$ is 14 000, and the emissivity is assumed to be 0·3 for both the melt and the solid. Much to our surprise, earth's gravitational field and ordinary zone travel rates were found to have negligible influence on the convection for silicon.

The results are not exact insofar as the assumed shape of the zone and the assumed heat-transfer conditions do not correspond precisely to experimental conditions. Nevertheless the results show the type and magnitude of the phenomena expected.

EQUATIONS

Incompressible axisymmetric steady state flow in the molten zone is assumed, with constant properties. The zone is taken to be a circular cylinder with planar solid–liquid interfaces and an aspect ratio l/a of unity (which are typical operating conditions, to the first approximation).* It was assumed that there was no crystal rotation. The pertinent differential equations and boundary conditions are as follows:

Momentum and continuity equations

$$\frac{\partial v_r}{\partial r}+\frac{v_r}{r}+\frac{\partial v_z}{\partial z}=0 \tag{1}$$

$$\rho\left(v_r\frac{\partial v_r}{\partial r}+v_z\frac{\partial v_r}{\partial z}\right)= -\frac{\partial P}{\partial r}+\mu\left(\frac{\partial^2 v_r}{\partial r^2}+\frac{1}{r}\frac{\partial v_r}{\partial r}-\frac{v_r}{r^2}+\frac{\partial^2 v_r}{\partial z^2}\right) \tag{2}$$

$$\rho\left(v_r\frac{\partial v_z}{\partial r}+v_z\frac{\partial v_z}{\partial z}\right)= -\frac{\partial P}{\partial z}+\mu\left(\frac{\partial^2 v_z}{\partial r^2}+\frac{1}{r}\frac{\partial v_z}{\partial r}+\frac{\partial^2 v_z}{\partial z^2}\right)-g \tag{3}$$

*On earth, the zone deviates from a cylindrical geometry primarily because of gravity, while in space the small variations in surface tension will cause small deviations in shape.

Boundary conditions are

(a) At $z = l$ (melting interface);

$$v_r = 0,\ v_z = -v_c\left(\frac{\rho_c}{\rho_f}\right)$$

(b) At $z = -l$ (freezing interface);

$$v_r = 0,\ v_z = -v_c\left(\frac{\rho_c}{\rho_f}\right)$$

(c) At $r = 0$ (along axial axis);

$$v_r = 0,\ \frac{\partial v_z}{\partial r} = 0$$

(d) At $r = a$ (free melt surface);

$$v_r = 0,\ \mu\frac{\partial v_z}{\partial r} = \frac{\partial \gamma}{\partial z}.$$

The pressure terms in the equations (2) and (3) are eliminated to obtain the momentum and continuity equations in the form of stream function, ψ, as follows:

$$\begin{aligned}&\frac{1}{R}\frac{\partial\psi}{\partial Z}\left(\frac{\partial^3\psi}{\partial Z^2\partial R}-\frac{1}{R}\frac{\partial^2\psi}{\partial Z^2}+\frac{\partial^3\psi}{\partial R^3}-\frac{2}{R}\frac{\partial^2\psi}{\partial R^2}+\frac{2}{R^2}\frac{\partial\psi}{\partial R}\right)\\&-\frac{1}{R}\frac{\partial\psi}{\partial R}\frac{\partial}{\partial Z}\left(\frac{\partial^2\psi}{\partial Z^2}+\frac{\partial^2\psi}{\partial R^2}-\frac{1}{R}\frac{\partial\psi}{\partial R}\right)-\frac{1}{R^2}\frac{\partial\psi}{\partial Z}\frac{\partial^2\psi}{\partial Z^2}\\&+\frac{1}{R^2}\frac{\partial\psi}{\partial Z}\left(-\frac{\partial^2\psi}{\partial R^2}+\frac{1}{R}\frac{\partial\psi}{\partial R}\right)\\&-\left(2\frac{\partial^4\psi}{\partial Z^2\partial R^2}-\frac{2}{R}\frac{\partial^3\psi}{\partial Z^2\partial R}+\frac{\partial^4\psi}{\partial Z^4}+\frac{\partial^4\psi}{\partial R^4}-\frac{2}{R}\frac{\partial^3\psi}{\partial R^3}\right.\\&\left.+\frac{3}{R^2}\frac{\partial^2\psi}{\partial R^2}-\frac{3}{R^3}\frac{\partial\psi}{\partial R}\right)\\&+Gr_h(\partial\theta/\partial R)+Gr_m(\partial\Phi/\partial R)=0.\end{aligned}\quad(4)$$

The boundary conditions in the form of stream function are:

(a) At $Z = l/a$; $\dfrac{\partial\psi}{\partial Z} = 0,\ \psi = \dfrac{R^2V_c}{2}\left(\dfrac{\rho_c}{\rho_f}\right)$

(b) At $Z = -l/a$; $\dfrac{\partial\psi}{\partial Z} = 0,\ \psi = \dfrac{R^2V_c}{2}\left(\dfrac{\rho_c}{\rho_f}\right)$

(c) At $R = 0$; $\psi = 0$,* $\dfrac{\partial\psi}{\partial R} = 0$

(d) At $R = 1$; $\psi = \dfrac{V_c}{2}\left(\dfrac{\rho_c}{\rho_f}\right),\ \dfrac{\partial\psi}{\partial R}-\dfrac{\partial^2\psi}{\partial R^2} = M\dfrac{\partial\theta}{\partial Z}$

Heat-transfer equations

If the thermal properties are constant and the viscous dissipation is neglected, the differential equation for heat transfer is:

$$\rho C_p\left(v_z\frac{\partial T}{\partial z}+v_r\frac{\partial T}{\partial r}\right)=k\left(\frac{\partial^2T}{\partial z^2}+\frac{1}{r}\frac{\partial T}{\partial r}+\frac{\partial^2T}{\partial r^2}\right).\quad(5)$$

*The stream function at the Z-axis is an arbitrary constant and is taken to be zero.

The boundary conditions for heat transfer are:

(a) At $r = 0$; $\dfrac{\partial T}{\partial r} = 0$

(b) At $r = a$; $-k\dfrac{\partial T}{\partial r} = \sigma\varepsilon_s(T^4 - T_c^4)$

(c) At $\begin{cases} r = a \\ z = 0 \end{cases}$; $T = T_0$ (ring heat source)

(d) At $z = l$; $T = T_m$

(e) At $z = -l$; $T = T_m$.

The above equations are restated in the following dimensionless form:

$$V_z\frac{\partial\theta}{\partial Z}+V_r\frac{\partial\theta}{\partial R}=\frac{1}{Pr}\left(\frac{\partial^2\theta}{\partial Z^2}+\frac{1}{R}\frac{\partial\theta}{\theta R}+\frac{\partial^2\theta}{\partial R^2}\right).\quad(6)$$

The boundary conditions in dimensionless form are

(a) At $R = 0$; $\dfrac{\partial\theta}{\partial R} = 0$

(b) At $R = 1$;

$$\frac{\partial\theta}{\partial R} = -\frac{a\sigma\varepsilon_s}{k\Delta T}\left[\{\theta\Delta T+T_m\}^4-\{\theta_c\Delta T+T_m\}^4\right]$$

(c) At $\begin{cases} R = 1 \\ Z = 0 \end{cases}$; $\theta = \dfrac{T_0 - T_m}{\Delta T}$

(d) At $Z = l/a$; $\theta = 0$

(e) At $Z = -l/a$; $\theta = 0$.

Of the above boundary conditions for momentum and heat transfer, only those applied at the free melt surface should require any explanation. No material transfer normal to the surface is assumed; hence v_r is zero. A balance in the stresses of viscous shear and surface tension gradient leads to the latter portion of boundary condition (4)d. The heat-transfer boundary conditions (6)b and c apply only to the problems with a ring heat source.

For the parabolic temperature profiles with a zone aspect ratio of one (i.e. $a = l$), the following dimensionless parabolic temperature profile equation is used in place of boundary conditions (6)b and c.

$$\theta = 1 - Z^2.\quad(7)$$

The flow field is symmetrical about the $z = 0$ axis for a stationary zone at zero gravity. This was tested by using the boundary condition at the solid/melt interface ($z = -l$) in place of the symmetry boundary condition at $z = 0$.

Mass-transfer equations

The differential equation for mass transfer of the impurity is

$$v_z\frac{\partial w}{\partial z}+v_r\frac{\partial w}{\partial r}=D\left(\frac{\partial^2w}{\partial z^2}+\frac{1}{r}\frac{\partial w}{\partial r}+\frac{\partial^2w}{\partial r^2}\right).\quad(8)$$

Table 1. Summary of the dependence of convection on operating conditions

M	Gr_h	v_c (cm/h)	Pr	Grid ($n \times m$)	Maximum dimensionless velocity component of fluid and its location	Maximum vorticity and its location	Cell centers, location and direction of rotation (+) for clockwise (−) for counterclockwise 1st	2nd	3rd	4th	Cell symmetrical about
					Heating method: parabolic T profile (radiant heating)						
35	0	0	0·023	11 × 11	$V_z = 5{\cdot}8$ $Z = 0{\cdot}7$ $R = 1$	$\omega = 212$ $Z = 1$ $R = 0{\cdot}9$	(−) $Z = 0{\cdot}65$ $R = 0{\cdot}81$				R and Z axis
350	0	0	0·023	11 × 11	$V_z = 62{\cdot}3$ $Z = 0{\cdot}7$ $R = 1$	$\omega = 2352$ $Z = 1$ $R = 0{\cdot}9$	(−) $Z = 0{\cdot}7$ $R = 0{\cdot}83$				R and Z axis
3500	0	0	0·023	21 × 21	$V_z = 219$ $Z = 0{\cdot}85$ $R = 1$	$\omega = 15\,510$ $Z = 1$ $R = 0{\cdot}9$	(−) $Z = 0{\cdot}86$ $R = 0{\cdot}79$	(+) $Z = 0{\cdot}34$ $R = 0{\cdot}50$			R and Z axis
7000	0	0	0·023	41 × 41	$V_z = 275$ $Z = 0{\cdot}9$ $R = 1$	$\omega = 28\,850$ $Z = 1$ $R = 0{\cdot}95$	(−) $Z = 0{\cdot}88$ $R = 0{\cdot}92$	(+) $Z = 0{\cdot}63$ $R = 0{\cdot}72$	(−) $Z = 0{\cdot}65$ $R = 0{\cdot}52$	(+) $Z = 0{\cdot}62$ $R = 0{\cdot}35$	R and Z axis
					Heating method: ring heat source (electron beam heating)						
350	0	0	0·023	11 × 21	$V_r = 77$ $Z = 0$ $R = 0{\cdot}9$	$\omega = 2402$ $Z = 0{\cdot}1$ $R = 0{\cdot}9$	(−) $Z = 0{\cdot}1$ $R = 0{\cdot}9$	(−) $Z = 0{\cdot}48$ $R = 0{\cdot}79$			R and Z axis
350	0	1–5	0·023	11 × 21	Almost the same as the case of $M = 350$, $V_c = 0$ and electron beam heating						
350	0	5	0·023	21 × 41	$V_r = 69$ $Z = 0$ $R = 0{\cdot}95$	$\omega = 3982$ $Z = 0{\cdot}05$ $R = 0{\cdot}95$	(−) $Z = 0{\cdot}05$ $R = 0{\cdot}95$	(−) $Z = 0{\cdot}05$ $R = 0{\cdot}95$			R and Z axis
350	0	1	0·30	11 × 21	$V_r = 67$ $Z = 0$ $R = 0{\cdot}9$	$\omega = 2091$ $Z = 0{\cdot}1$ $R = 0{\cdot}9$	(−) $Z = 0{\cdot}1$ $R = 0{\cdot}9$	(−) $Z = 0{\cdot}7$ $R = 0{\cdot}8$			R and Z axis
350	0	1	2·0	11 × 21	$V_r = 92$ $Z = 0$ $R = 0{\cdot}9$	$\omega = 3192$ $Z = 0{\cdot}1$ $R = 0{\cdot}9$	(−) $Z = 0{\cdot}1$ $R = 0{\cdot}9$	(−) $Z = 0{\cdot}9$ $R = 0{\cdot}88$			R and Z axis
35	0	0	0·023	11 × 21	$V_r = 9{\cdot}7$ $Z = 0$ $R = 0{\cdot}9$	$\omega = 265$ $Z = 0{\cdot}1$ $R = 0{\cdot}9$	(−) $Z = 0{\cdot}1$ $R = 0{\cdot}89$				R and Z axis

Table 1—*Continued*

M	Gr_h	v_c (cm/h)	Pr	Grid ($n \times m$)	Maximum dimensionless velocity component of fluid and its location	Maximum vorticity and its location	Cell centers, location and direction of rotation (+) for clockwise (−) for counterclockwise 1st	2nd	3rd	4th	Cell symmetrical about
35	0	10	0·023	11 × 21	$V_r = 9{\cdot}6$ $Z = 0$	$\omega = 266$ $Z = 0{\cdot}1$	(−) $Z = 0{\cdot}1$ $R = 0{\cdot}9$				
					$R = 0{\cdot}9$	$R = 0{\cdot}9$	(+) $Z = -0{\cdot}1$ $R = 0{\cdot}9$				Z axis
35	0	30	0·023	11 × 21	$V_r = 9{\cdot}7$ $Z = 0$	$\omega = 266$ $Z = 0{\cdot}1$	(−) $Z = 0{\cdot}1$ $R = 0{\cdot}9$				
					$R = 0{\cdot}9$	$R = 0{\cdot}9$	(+) $Z = -0{\cdot}3$ $R = 0{\cdot}7$				Z axis
35	0	50	0·023	11 × 21	$V_r = 9{\cdot}7$ $Z = 0$	$\omega = 328$ $Z = 1{\cdot}0$	(−) $Z = 0{\cdot}1$ $R = 0{\cdot}9$				
					$R = 0{\cdot}9$	$R = 0{\cdot}9$	(+) $Z = -0{\cdot}34$ $R = 0{\cdot}62$				Z axis
35	0	70	0·023	11 × 21	$V_r = 9{\cdot}7$ $Z = 0$	$\omega = 432$ $Z = 1$	(−) $Z = 0{\cdot}1$ $R = 0{\cdot}9$				
					$R = 0{\cdot}9$	$R = 0{\cdot}9$	(+) $Z = -0{\cdot}37$ $R = 0{\cdot}56$				Z axis
350	77·5	1	0·023	11 × 21	Almost the same as for $v_c = 0$						Z axis
350	775	1	0·023	11 × 21	$V_r = 78$ $Z = 0$	$\omega = 2374$ $Z = 0{\cdot}1$	(−) $Z = 0{\cdot}1$ $R = 0{\cdot}9$	(−) $Z = 0{\cdot}3$ $R = 0{\cdot}77$			
					$R = 0{\cdot}9$	$R = 0{\cdot}9$	(+) $Z = -0{\cdot}1$ $R = 0{\cdot}9$	(+) $Z = -0{\cdot}6$ $R = 0{\cdot}9$			Z axis

The boundary conditions are

(a) At $r = 0$; $\dfrac{\partial w}{\partial r} = 0$

(b) At $r = a$; $\dfrac{\partial w}{\partial r} = 0$

(c) At $z = -l$; $k_0 w v_c = w v_c \left(\dfrac{\rho_c}{\rho_f}\right) + D\left(\dfrac{\mathrm{d}w}{\mathrm{d}z}\right)$

(d) At $z = l$; $w_0 v_c = w v_c \left(\dfrac{\rho_c}{\rho_f}\right) + D\left(\dfrac{\mathrm{d}w}{\mathrm{d}z}\right)$

where k_0 is the ratio of impurity concentration in solid to that in melt at the freezing interface (usually determined from the phase diagram). The last two equations of boundary condition are derived from the interfacial material balance for the impurity [2].

The above equations are restated in the following dimensionless forms:

$$V_z \frac{\partial \Phi}{\partial Z} + V_r \frac{\partial \Phi}{\partial R} = \frac{1}{Sc}\left[\frac{\partial^2 \Phi}{\partial R^2} + \frac{1}{R}\frac{\partial \Phi}{\partial R} + \frac{\partial^2 \Phi}{\partial Z^2}\right]. \quad (9)$$

Boundary conditions

(a) At $R = 0$; $\dfrac{\partial \Phi}{\partial R} = 0$

(b) At $R = 1$; $\dfrac{\partial \Phi}{\partial R} = 0$

(c) At $Z = -\dfrac{l}{a}$; $k_0 \Phi V_c = \Phi V_c \left(\dfrac{\rho_c}{\rho_f}\right) + \dfrac{1}{Sc}\dfrac{\mathrm{d}\Phi}{\mathrm{d}Z}$

(d) At $Z = \dfrac{l}{a}$; $V_c = \Phi V_c \left(\dfrac{\rho_c}{\rho_f}\right) + \dfrac{1}{Sc}\dfrac{\mathrm{d}\Phi}{\mathrm{d}Z}$.

COMPUTATION

One of the typical numerical procedures for calculating the stream function in an enclosed fluid is to solve for the vorticity function by a successive iteration method [4–6] and then find the stream function from vorticity. Rather than finding the stream function via the vorticity equation to compute the stream function, we used equation (4) in a single step. An approximate solution was obtained at a finite number of equidistant grid points having coordinates $Z = (i-1)\Delta Z$ and $R = (j-1)\Delta R$, where i and j are integers. The grid points $(n \times m)$ cover the region from the z-axis to the free melt surface in the r-direction and from the bottom interface to the top interface in the z-direction with the ring heat sources. With the parabolic temperature profiles, however, a symmetrical flow about the r-axis is assumed and $n \times m$ covers only the mirror image in the top half. The central finite difference method (which is synonymous to the parabolic finite difference method in some literature) was employed for equation (4), and the development of the approximate equations are illustrated in Appendix A. The resultant computation molecule is shown in Fig. 2, in which twelve current values at the nearest neighboring grid points are required for an explicit computation of the new stream function. Computations of the stream function at the grid points next to the liquid/solid interfaces and to the axis were made using the boundary conditions. The stream functions at the interior grid points next to the free liquid surface were calculated by the interpolation method. The Gauss–Seidel iteration method [7] was employed for computer calculation. For $M < 350$ we obtained convergent solutions when 11×11 grid points were used. However, an increased number of grid points were necessary for convergence with higher values of M, as shown in Table 1 where the results are summarized.

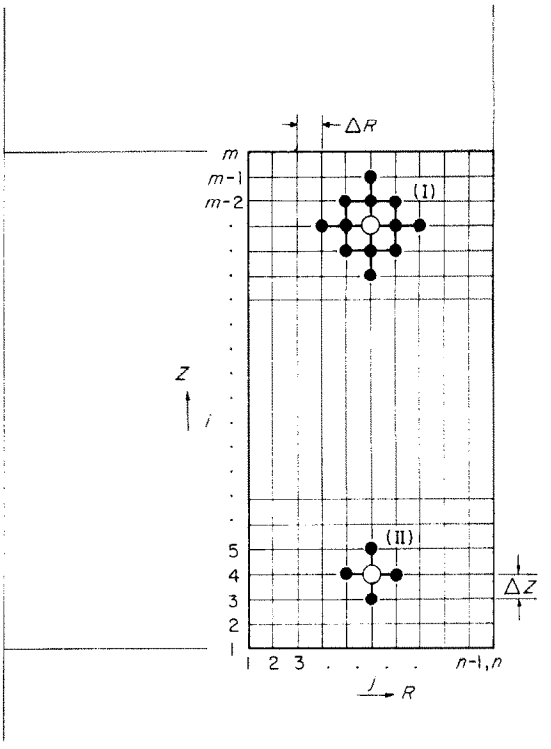

FIG. 2. The finite difference grid system and the computational molecules used in the numerical calculations [(I) for stream function, (II) for temperature and concentration].

Dimensionless vorticities and velocities in the melt were computed from the stream function results. The calculated flow velocities were utilized for computations of the temperature and impurity concentration fields. The same computational scheme was employed for the analysis of heat and mass transfer. The finite difference forms of equation (6) for heat transfer, and of equation (9) for mass transfer resulted in the computation molecule as shown in Fig. 2. The Newton–Raphson method [7] was used to iteratively solve for the temperatures at the surfaces because of the nonlinearity of the thermal radiation boundary conditions. A rapidly converging solution for heat transfer was attained by using overrelaxation parameter of 1·9 when the Prandtl number was low (metals). In heat-transfer analyses with high Prandtl number or in mass-transfer analyses for high Schmidt number liquids (including silicon), introduction of the overrelaxation parameter impaired the convergence. An underrelaxation parameter had to be employed in order to obtain a convergent solution, at the expense of an increased number of iterations.

Convergence and accuracy tests were carried out: (1) by increasing the number of iterations with a more stringent accuracy limit, and (2) by increasing the number of grid points for an identical problem. For example, the former test showed that there was no essential change in the solution with an increased number of iterations. The latter test also showed no great difference in the flow patterns and in the profiles of temperature and concentration fields, except that the concentration field becomes smoother when M is 350. The vortex center near the heat source does tend to be associated with an individual grid point. However, this tendency does not influence the flow pattern or flow intensity elsewhere. The results of the grid refinement test for $M = 350$ are compared in Table 1 and in Figs. 6(a) and (b).

RESULTS

Streamlines for a parabolic temperature profile at the free melt surface (radiation heating)

For simplicity, a parabolic temperature profile along the melt surface was assumed for our initial calculations. This enabled us to solve the momentum equations without simultaneously solving the heat-transfer equations. A parabolic profile, with a maximum at the center, seems reasonable for radiant heating. The dimensionless surface tension parameter M decreases as the radius of the zone "a" and the temperature variation along the melt surface increases.

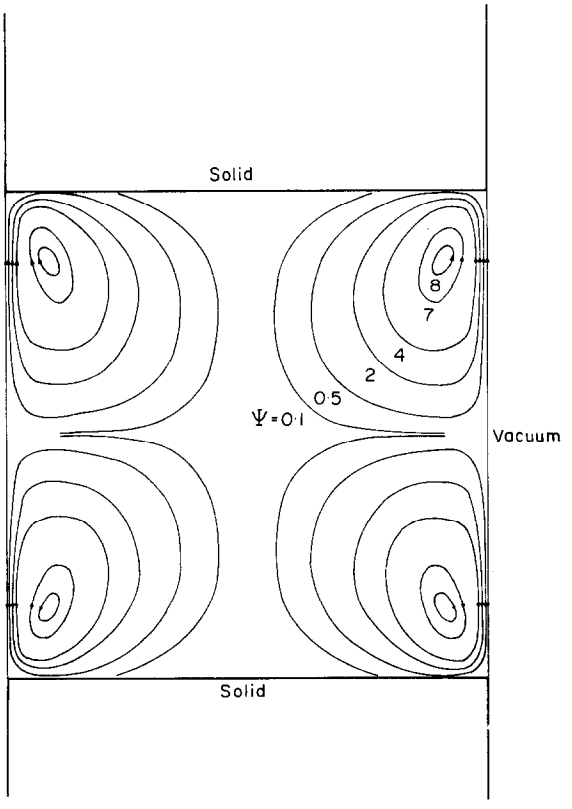

FIG. 3. Computed dimensionless streamlines ψ for surface tension driven flow in a floating zone at zero gravity with a parabolic temperature profile on the free liquid surface with $M = 350$ and $v_c = 0$. For silicon with $(T_0 - T_m) = 0{\cdot}05°C$ and $a = 0{\cdot}5$ cm.

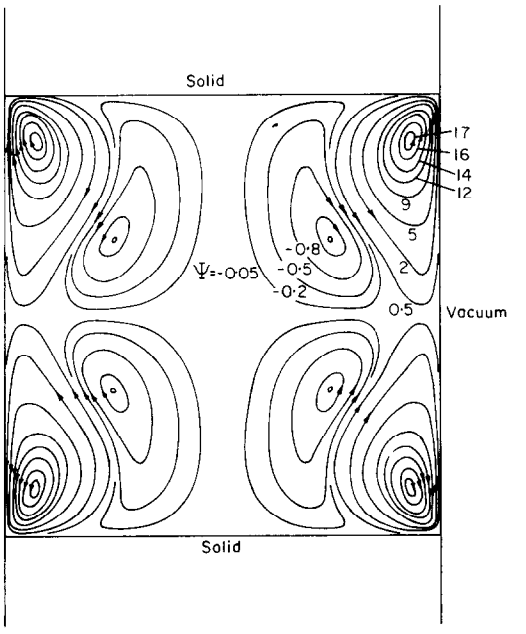

FIG. 4. Computed dimensionless streamlines ψ for surface tension driven flow in a floating zone at zero gravity with a parabolic temperature profile on the free liquid surface with $M = 3500$ and $v_c = 0$. Silicon with $(T_0 - T_m) = 0{\cdot}5°C$ and $a = 0{\cdot}5$ cm.

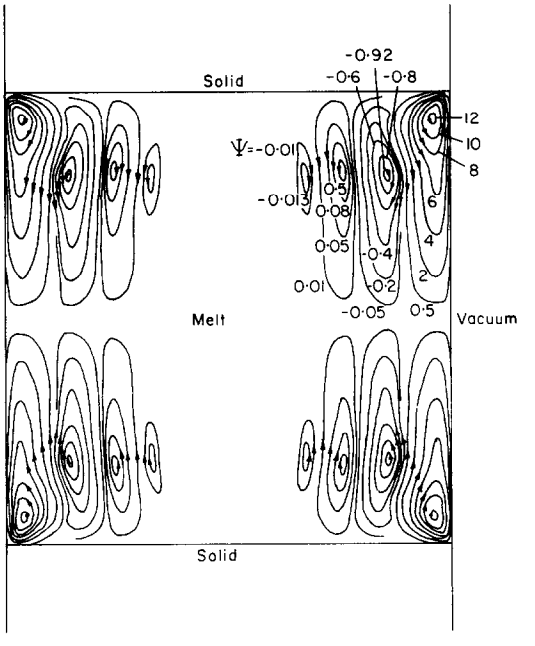

FIG. 5. Computed dimensionless streamlines ψ for surface tension driven flow in a floating zone at zero gravity with a parabolic temperature profile on the free liquid surface with $M = 7000$ and $v_c = 0$. Silicon with $(T_0 - T_m) = 1{\cdot}0°C$ and $a = 0{\cdot}5$ cm.

In Figs. 3–5, the streamlines for parabolic temperature profiles are shown to illustrate the effect of increased values of M (350, 3500 and 7000). Donut-shaped vortex cells were formed. With $M = 35$ and 350 only two cells are generated, and the centers of the vortices move closer toward the liquid/solid interfaces as M increases.

With $M = 3500$, however, which corresponds to a condition of $a = 0{\cdot}5$ cm and $(T_0 - T_m) = 0{\cdot}5$°C for silicon,* secondary vortex cells were induced behind the primary vortex, as shown in Fig. 4. As the value of M was further increased up to 7000, third and fourth vortices were produced, as shown in Fig. 5. These multiple vortices are probably indicative of oscillations and incipient turbulence, which cannot be calculated in a steady state analysis (oscillations are frequently found with free convection in enclosed cavities between laminar and fully turbulent flow). The maximum velocity of the melt for 1 cm dia silicon with $(T - T_m) = 1{\cdot}0$°C is calculated to be 2 cm/sec.

Fluid flow coupled with heat transfer (electron beam heating)

Electron beam heating is commonly used in floating zone melting and was considered as another heating mode. A ring heat source at the center of the zone ($z = 0$) was assumed. Rather than specify the power input, the circumferential temperature T_0 at the center of the zone was specified for convenience in analysis. The procedure used to solve the coupled heat-momentum transport problem was as follows.

(1) The temperature field for conduction was computed by neglecting convective heat transfer.

(2) The surface temperature profile from (1) was utilized to calculate the first approximate solution of fluid flow.

(3) The temperature field was recalculated using the flow fields from (2).

(4) Steps (2) and (3) were repeated until the temperature and the fluid flow fields no longer changed appreciably.

The resulting streamlines with $M = 350$† are drawn in Fig. 6 in which we took values for silicon with the surroundings at the melting point, i.e. the heat shielding about the zone is extremely effective. While this does not correspond exactly with reality, it does show the correct features. Comparing with Fig. 3, we see that the vortex centers are shifted nearer to the heat source from the liquid–solid interfaces. This is because the steepest temperature gradient is at the center of the zone. The maximum velocity for silicon was 0·55 cm/s. Comparing the temperature fields with surface tension driven flow for $M = 350$ with those for pure conduction, there was no significant change except for a slight one near the center of the zone. This indicates that conduction is much greater than convective heat transfer as would be expected for the small Prandtl number for silicon. The vorticity fields for $M = 350$ are shown in Fig. 7. The maximum vorticity and its location for various conditions are also summarized in Table 1.

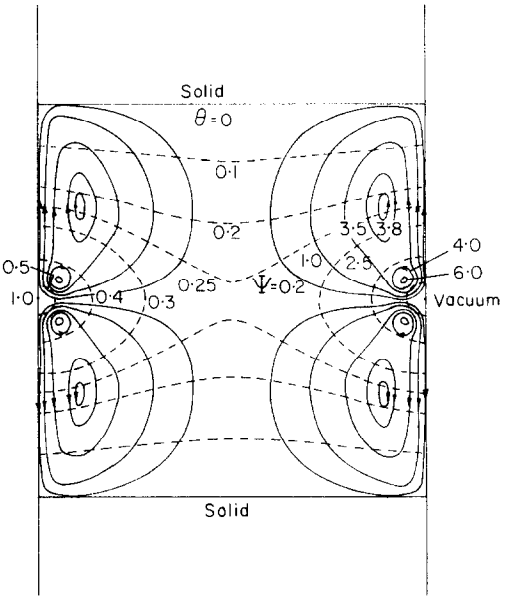

FIG. 6(a). Isotherms θ and streamlines ψ at zero gravity for electron beam heating of silicon with $(T_0 - T_m) = 0{\cdot}05$°C, $T_c = T_m$, $\varepsilon_s = 0{\cdot}3$, $a = 0{\cdot}5$ cm, $M = 350$, $Pr = 0{\cdot}023$, $v_c = 0$. Calculation performed with 11 × 21 grid.

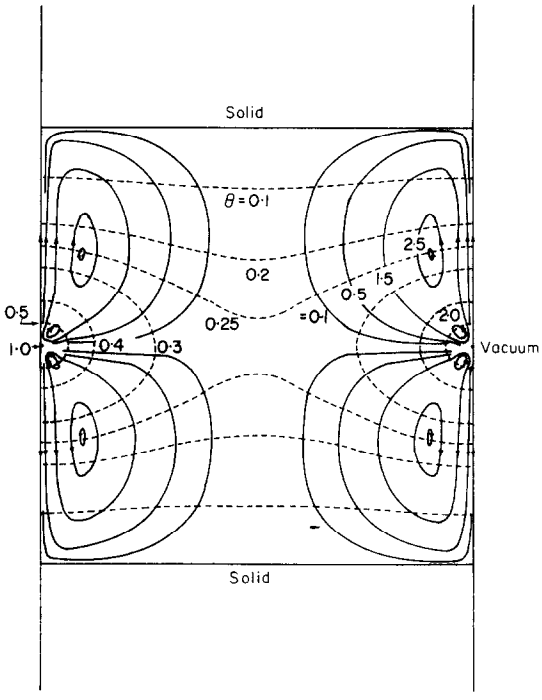

FIG. 6(b). Isotherms θ and streamlines ψ for the same conditions as in Fig. 6(a). Calculation performed with 21 × 41 grid.

Influence of gravity on flow

In a vertical silicon melt with $M = 350$ at earth's gravity the flow and temperature fields in the floating zone do not change appreciably from those at zero g.*

*Without heat shielding, i.e. without thermal radiation reflectors about the zone or an auxiliary furnace, we estimate the temperature difference $(T_0 - T_m)$ would be on the order of 10–20°C, and the flow would be turbulent.

†For electron beam heating of 1 cm dia silicon, the Marangoni number Ma is about 1/50 of the value of M. Without heat shielding Ma is estimated to be about 60 000.

*Only temperature variations were considered.

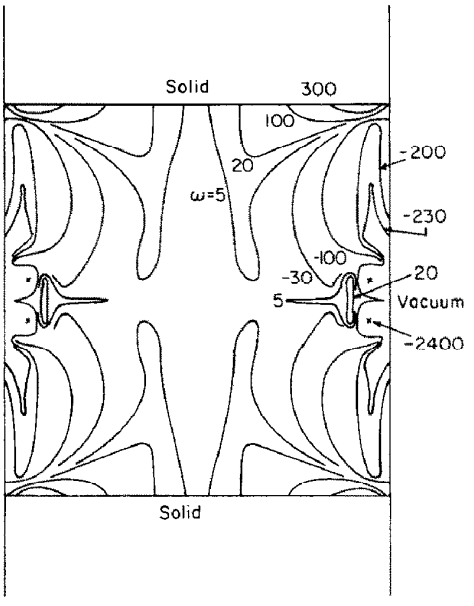

FIG. 7. Dimensionless vorticity field ω corresponding to the streamline field shown in Fig. 6(a).

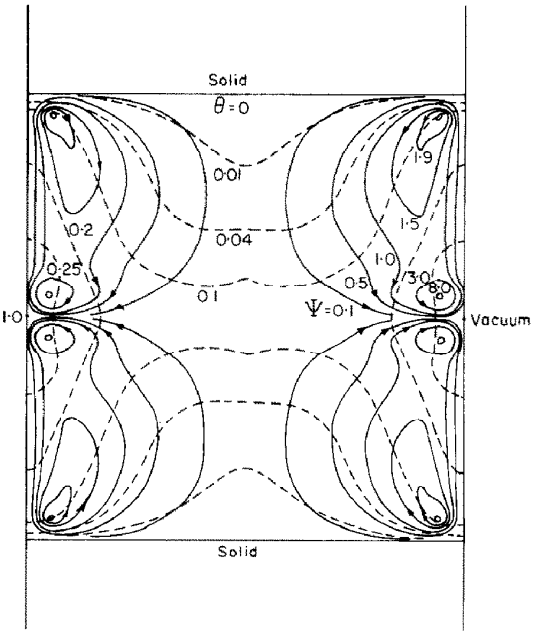

FIG. 9. Isotherms θ and streamlines ψ for the same conditions as in Fig. 6(a), except $Pr = 2$.

When the acceleration is increased to ten times the earth's gravity, the lower vortex contracts while the upper one is expanded, particularly at the center of the zone where the flow field is relatively weak. This is shown in Fig. 8 and may be compared with Fig. 6 at zero g. This means that surface driven flow predominates even on earth for many materials for radiant and electron beam heating. It may even be important when induction heating is employed and may account for some of the compositional inhomogeneities observed.

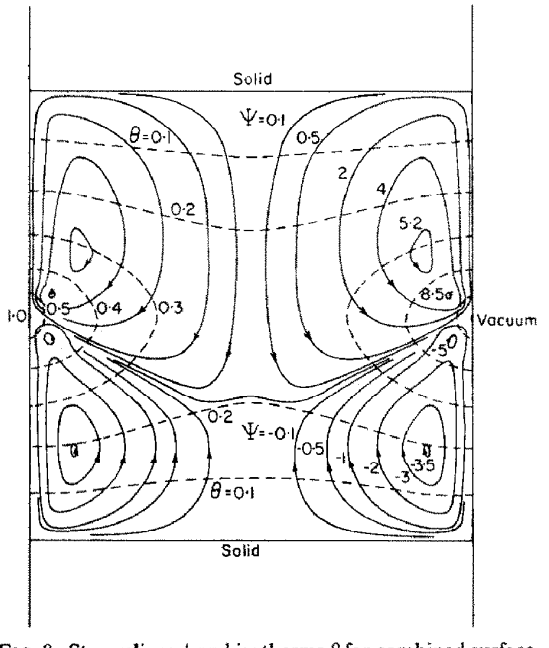

FIG. 8. Streamlines ψ and isotherms θ for combined surface-driven and buoyancy-driven flow with $Gr_h = 775$. Other conditions are the same as Fig. 6(a).

Influence of Prandtl number

The Prandtl number was increased from 0·023 to 0·3 and 2·0 by increasing the specific heat, and keeping the viscosity and the thermal conductivity of the melt constant. As the Prandtl number increases, the temperature gradients along the free liquid surface (for fixed $T_0 - T_m$) increase near the heat source and also near the liquid–solid interfaces, but decrease significantly in between. Since the convective heat transfer becomes more significant as a result of increasing the Prandtl number, the isotherms are increasingly distorted from those of pure conduction. This, in turn, causes changes in the flow field. For example, the center of the vortex cell near the liquid–solid interface shifts closer to the interface as the Prandtl number increases, as shown in Fig. 9.

Influence of zone travel on hydrodynamics

The effect of zone motion on the flow field was found to be negligible in all of our calculated streamlines for zone travel rates of up to 5 cm/h in silicon.* However, the effect becomes significant when the zone travel rate becomes comparable with the velocity of surface-driven flow.

The flow field for electron beam heating with $M = 35$ is taken as a model case in order to show the influence of zone travel on hydrodynamics in the floating zone. The maximum velocity of the melt for $M = 35$ is 0·07 cm/s (or 250 cm/h), and the average velocity is about 70 cm/h. In Fig. 10, the streamlines in floating zone melting of silicon at zero g are shown for a freezing rate of 30 cm/h. The lower vortex cell floats away from the bottom interface and its size is reduced as the zone travel rate increases.

*A zone travel rate of 5 cm/h is typical for growth of single crystals, while faster rates are employed for vacuum outgassing and lower rates for zone refining.

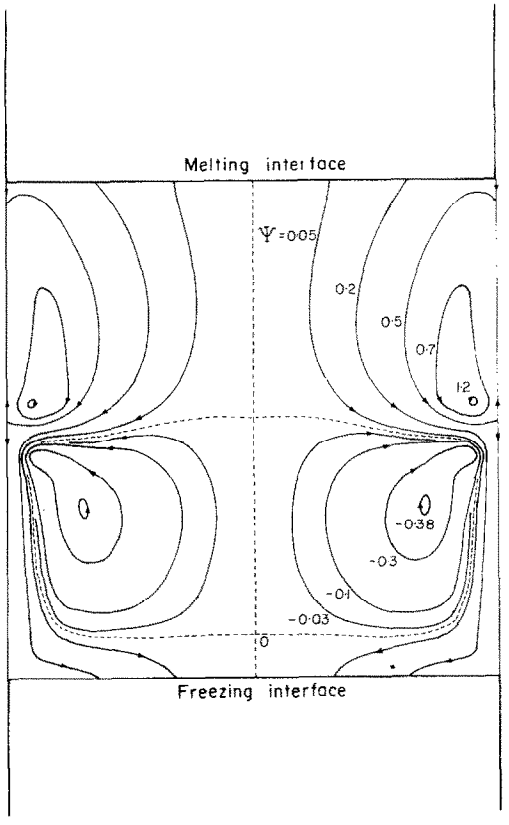

FIG. 10. Streamlines ψ at a zone travel rate of 30 cm/h with $M = 35$, $Pr = 0{\cdot}023$. For silicon, $a = 0{\cdot}5$ cm, $(T_0 - T_m) = 0{\cdot}005$°C, $T_c = T_m$, $\varepsilon_s = 0{\cdot}3$.

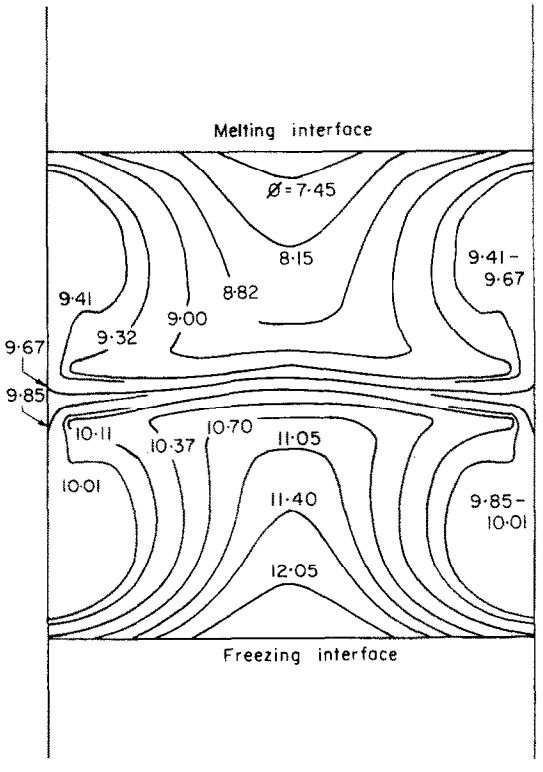

FIG. 11. Impurity concentration fields Φ in a silicon melt at steady state for a zone travel rate of $v_c = 5$ cm/h, $M = 350$, $Pr = 0{\cdot}023$, $Sc = 5{\cdot}0$, $k_0 = 0{\cdot}1$, $D = 7{\cdot}6 \times 10^{-4}$ cm^2/s, $a = 0{\cdot}5$ cm. Calculation performed with 21 × 41 grid.

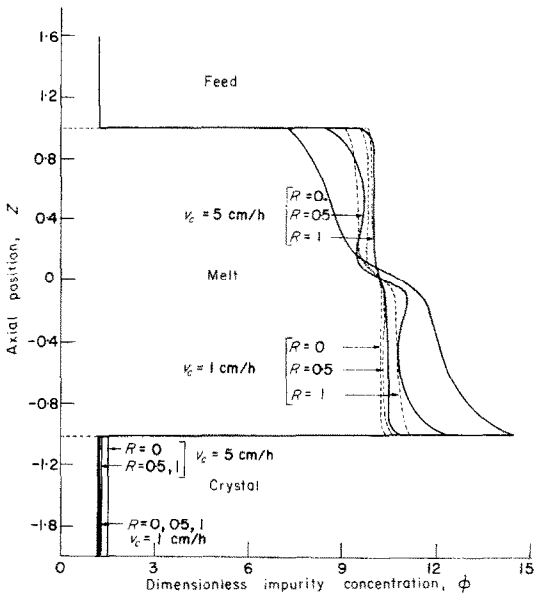

FIG. 12. Impurity concentration profiles in the axial direction at $R = 0$, 0·5 and 1·0 under the same conditions as Fig. 11.

Impurity segregation

Steady state* impurity concentration fields in the melt were calculated by introducing the convection fields for $M = 350$ with zone motion. The values used in the present computations are: $Sc = 5{\cdot}0$, $\rho_c = 2{\cdot}28$ g/cm^3, $\rho_f = 2{\cdot}54$ g/cm^3, $k_0 = 0{\cdot}1$, $a = 0{\cdot}5$ cm and $D = 7{\cdot}6 \times 10^{-4}$ cm^2/s, which are typical for silicon with aluminum or indium impurity. The dimensionless impurity concentration fields at steady state are shown in Fig. 11 for a freezing rate v_c of 5 cm/h ($V_c = 0{\cdot}183$). The dimensionless impurity concentration profiles in the axial direction at $R = 0$, 0·5 and 1·0 are plotted in Fig. 12 for freezing rates of 1 cm/h and 5 cm/h. The magnitude of the mass-transfer resistance is indicated by the rate of change of concentration with distance. Note that it is higher at the center of the zone because of the poor mixing between the top and bottom cells. This is to be contrasted with boundary-layer flow in which the mass-transfer resistance is concentrated near solid–liquid interfaces.

CONCLUSION

For silicon we have seen that surface tension driven flow is very vigorous, and is turbulent when heat shields are not employed. The buoyancy flow is negligible in comparison. With moderate heat shielding, oscillatory convection is likely, but was not studied here. Zone motion does not have an appreciable effect on the convection unless the temperature gradients along the melt surface are made very small by effective heat shielding. With laminar flow, the convection has only

*When zone melting is initiated the impurity concentration in the melt increases (for $k_0 < 1$) until the same average concentration is freezing out of the melt as is being fed into the melt at the other interface. It takes several zone lengths of zone movement with convective mixing in the zone until this steady state is reached.

a small influence on heat transfer at small Prandtl number ($Pr \ll 1$), but a large influence for $Pr > 1$. The laminar flow cells would lead to significant inhomogeneities in the melt during zone melting. This, in turn, would cause inhomogeneities in the resulting crystals.

Acknowledgements—This research was supported by the National Aeronautics and Space Administration under Contract NAS8-29847 and by the National Science Foundation under Grant GK-40792. We are grateful to Tommy Bannister, Stewart Churchill and Simon Ostrach for their advice and encouragement.

REFERENCES

1. W. G. Pfann, *Zone Melting*, 2nd edn. Wiley, New York (1960).
2. M. Zief and W. R. Wilcox, editors, *Fractional Solidification*. Dekker, New York (1967).
3. W. R. Wilcox, Crystallization flow, *J. Crystal Growth* **12**, 93–96 (1972).
4. J. O. Wilkes and S. W. Churchill, The finite-difference computation of natural convection in a rectangular enclosure, *A.I.Ch.E. Jl* **12**, 161 (1966).
5. L. C. Tien, Freezing of a convective liquid in a crystal-growth tube, Ph.D. Thesis, University of Michigan, Ann Arbor (1969).
6. K. E. Torrance, L. Orloff and J. A. Rockett, Numerical study of natural convection in an enclosure with localized heating from below—creeping flow to the onset of laminar instability, *J. Fluid Mech.* **36**, 33 (1969).
7. B. W. Arden and K. N. Astill, *Numerical Algorithms: Origin and Applications*. Addison-Wesley, Reading, Mass. (1970).

APPENDIX

Finite-Difference Scheme for Momentum Equation

(I) The following approximations are used for the equation (4).

$$\frac{\partial\psi}{\partial Z} = \frac{\psi_{i+1,j}-\psi_{i-1,j}}{2(\Delta Z)}$$

$$\frac{\partial\psi}{\partial R} = \frac{\psi_{i,j+1}-\psi_{i,j-1}}{2(\Delta R)}$$

$$\frac{\partial^2\psi}{\partial Z^2} = \frac{\psi_{i+1,j}-2\psi_{i,j}+\psi_{i-1,j}}{(\Delta Z)^2}$$

$$\frac{\partial^2\psi}{\partial R^2} = \frac{\psi_{i,j+1}-2\psi_{i,j}+\psi_{i,j-1}}{(\Delta R)^2}$$

$$\frac{\partial^2\psi}{\partial R\partial Z} = \frac{\psi_{i+1,j+1}-\psi_{i-1,j+1}-\psi_{i+1,j-1}+\psi_{i-1,j-1}}{4(\Delta R)(\Delta Z)}$$

$$\frac{\partial^3\psi}{\partial Z^3} = \frac{\psi_{i+2,j}-2\psi_{i+1,j}+2\psi_{i-1,j}-\psi_{i-2,j}}{2(\Delta Z)^3}$$

$$\frac{\partial^3\psi}{\partial R^3} = \frac{\psi_{i,j+2}-2\psi_{i,j+1}+2\psi_{i,j-1}-\psi_{i,j-2}}{2(\Delta R)^3}$$

$$\frac{\partial^4\psi}{\partial Z^4} = \frac{\psi_{i+2,j}-4\psi_{i+1,j}+6\psi_{i,j}-4\psi_{i-1,j}+\psi_{i-2,j}}{(\partial Z)^4}$$

$$\frac{\partial^4\psi}{\partial R^4} = \frac{\psi_{i,j+2}-4\psi_{i,j+1}+6\psi_{i,j}-4\psi_{i,j-1}+\psi_{i,j-2}}{(\Delta R)^4}$$

$$\frac{\partial^3\psi}{\partial R^2\partial Z} = \frac{\psi_{i+1,j+1}-\psi_{i-1,j+1}-2\psi_{i+1,j}+2\psi_{i-1,j}+\psi_{i+1,j-1}-\psi_{i-1,j-1}}{2(\Delta Z)(\Delta R)^2}$$

$$\frac{\partial^3\psi}{\partial Z^2\partial R} = \frac{\psi_{i+1,j+1}-\psi_{i+1,j-1}-2\psi_{i,j+1}+2\psi_{i,j-1}+\psi_{i-1,j+1}-\psi_{i-1,j-1}}{2(\Delta R)(\Delta Z)^2}$$

$$\frac{\partial^4\psi}{\partial R^2\partial Z^2} = \frac{1}{(\Delta R)^2(\Delta Z)^2}[\psi_{i+1,j+1}-2(\psi_{i+1,j}+\psi_{i-1,j}+\psi_{i,j+1}+\psi_{i,j-1})+4\psi_{i,j}+\psi_{i-1,j+1}+\psi_{i+1,j-1}+\psi_{i-1,j-1}].$$

(II) The following approximate equation is used for the equation of boundary condition of (4)d.

$$\frac{\partial\psi_{i,n}}{\partial R} = \frac{1}{2(\Delta R)^2-6(\Delta R)}\{(8\psi_{i,n-1}-\psi_{i,n-2})+4MZ(\Delta R)^2\}.$$

ANALYSE DE L'ECOULEMENT PROVOQUE PAR LA TENSION SUPERFICIELLE DANS UNE ZONE FLOTTANTE EN FUSION

Résumé—On étudie numériquement les équations aux dérivées partielles des transferts de chaleur et de quantité de mouvement, en régime permanent pour un écoulement provoqué par la tension superficielle dans un bain cylindrique suspendu entre deux tiges. On tient compte de façon approchée des chauffages par rayonnement et par bombardement électronique. Pour des faibles valeurs des forces de tension, un anneau tournant se forme dans la moitié supérieure de la zone avec son symétrique dans la moitié inférieure. Pour de plus grandes valeurs, il se forme des cellules secondaires qui doivent probablement prendre un mouvement oscillatoire. On étudie l'influence sur la convection du nombre de Prandtl, du mouvement de la zone, et de la gravité. La résistance au transfert massique laminaire est plus importante au centre de la zone qu'aux interfaces solide–liquide.

ANALYSE DER DURCH OBERFLÄCHENSPANNUNG ERZEUGTEN STRÖMUNG IM FLIESSZONENSCHMELZEN

Zusammenfassung—Für die von der Oberflächenspannung erzeugte Strömung in einer zylindrischen Schmelze zwischen zwei Stäben wurde eine numerische Lösung aufgrund der stationären Differentialgleichung für Wärme- und Stoffübergang angegeben. Strahlungsheizung und Elektronenstrahlheizung wurden näherungsweise berücksichtigt. Für kleine Werte der treibenden Kraft formte sich ein rotierender Ring in der oberen Hälfte der Zone und ein Spiegelbild in der unteren Hälfte. Bei größeren Antriebskräften ergaben sich sekundäre Zellen, die wahrscheinlich eine oszillierende Bewegung ausführen würden. Der Einfluß der Prandtlzahl, der Zonengeschwindigkeit und des Auftriebs auf die Konvektion wurde ebenfalls untersucht. Der Hauptwiderstand für den Stoffaustausch im Laminarregime ergab sich eher im Mittelpunkt der Zone als an der fest-flüssigen Schicht.

АНАЛИЗ ТЕЧЕНИЯ ПОД ДЕЙСТВИЕМ ПОВЕРХНОСТНОГО НАТЯЖЕНИЯ ПРИ ПЛАВЛЕНИИ ПОДВИЖНОЙ ЗОНЫ

Аннотация — Течение под действием поверхностного натяжения цилиндрического расплава, заключенного между двумя стержнями, исследовалось путем численного решения стационарных дифференциальных уравнений переноса тепла и количества движения. Лучистый нагрев и нагрев электронным лучом рассматривались приближенно. При небольших значениях движущей силы в верхней части зоны образовывалось одно вращающееся кольцо, а в нижней половине — его зеркальное отображение. При более высоких значениях движущей силы образуются вторичные элементы, претерпевающие, очевидно, колебательное движение. Изучалось также влияние числа Прандтля, движения зоны и подъемной силы на процесс конвекции. Основное сопротивление переносу массы при ламинарном режиме течения наблюдалось скорее в центре зоны, нежели на границах раздела твердое тело-жидкость.